Chapter 5

Facile Synthesis of Doped C_xN_y QDs as Photoluminescent Matrix for Direct Detection of Hydroquinone

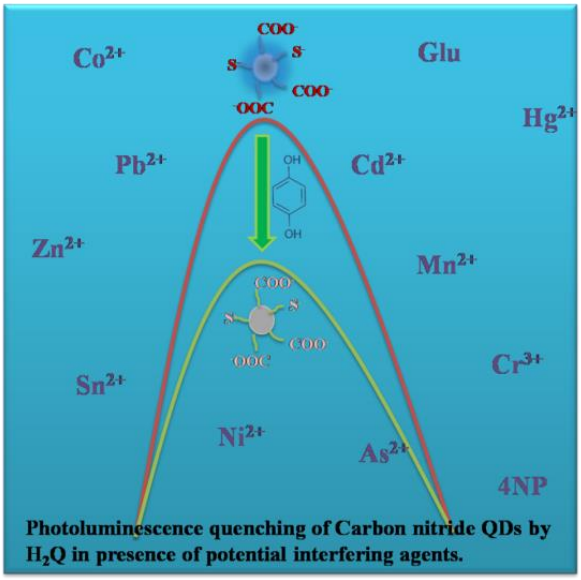

In this chapter, the Photochemical features of zero dimension of carbon nitride are discussed. We reported the facile hydrothermal synthesis of highly photoluminescent doped carbon nitride quantum dots (C_xN_y QDs) and implied it for direct detection of carcinogenic pollutant hydroquinone (H_2Q) by photoluminescence quenching phenomenon.

5.1 Introduction

Phenolic compounds are one of the organic pollutants which are released in water bodies as waste materials. These compounds are detrimental to aquatic bodies as well as aquatic species living in them. Hydroquinone (H_2Q) is one of them that is carcinogenic in nature and resistant to biotic and non-biotic degradations. [180,181] It is listed as a primary pollutant by European Union (EU) and US Environmental Protection Agency (EPA) because it produces ROS (reactive oxygen species) in the redox process which is cell damaging. [182,183] That is why, sensitive and selective detection of such pollutants is required to protect our ecosystem. Some detection methods like electrochemiluminescence (ECL), [184] high-performance liquid chromatography (HPLC), [185] gas chromatography (GC), [186] voltammetry, [187-189] flow injection analysis, [190] etc. are available in earlier reports, however, detection methods based on absorbance have many advantages over these ones due to quick response and high sensitivity. [191,192] Few reports are available on semiconducting QDs (e.g. CdSe QD) and its hybrid system (eg. CdTe QD-enzyme hybrid; Conjugated polymer-enzyme hybrid) for fluorescent detection of H_2Q. [193-195] However, these approaches have many disadvantages like complex sample preparation steps, enzyme denaturation and a high limit of detection.

Visible light active graphitic carbon nitride (g-C_3N_4) has been explored in a plethora of applications such as organic dye degradation, water splitting, supercapacitor application, H_2O_2 production, CO_2 and nitro reduction. [6,31,32] Carbon nitride at the nanometric level is an attractive destination because of its optical properties at zero dimension and one dimension level. Zero dimension of

graphitic carbon nitride exists as carbon nitride quantum dots (CNQDs). C_xN_y quantum dots term is used for the non-stoichiometric ratios of sp^2 hybridized carbon and nitrogen, where precursors used are not conventional as used in the preparation of g-C_3N_4. CNQDs are ahead of traditional semiconductors-based QDs owing to their low-cost synthesis, non-toxicity and environment friendliness. [17,18,21,91,196-200, 217] J. Chen et al. proposed the detection of hydroquinone using a combination of optical properties of graphitic carbon nitride quantum dots and specificity of enzymatic reaction. [20] There are two most prevailed precursors based on sources to prepare QDs (a) chemical and (b) biological precursors such as tree leaves, bark, etc. It involves doping of non-metals like O, N, P, S and B to enhance the fluorescence property of as-prepared QDs. These QDs are successfully used for heavy metals and biomolecules sensing either by colorimetric or fluorometric sensing methods. [201, 202]

Herein the present work, we are reporting the synthesis of photoluminescent O- and S-doped C_xN_y QDs by one-step hydrothermal treatment with the help of cheap and bio-compatible precursors namely cysteine and maleic acid in optimum ratios at 150°C. Here, cysteine is used as a source of nitrogen and also provides dopant S; while maleic acid serves as stabilizing agent due to the presence of carboxyl groups. The as-synthesized QD has high stability in aqueous media owing to its negatively charged surface. After that, it is further implied in sensitive and selective detection of H_2Q by photoluminescence quenching phenomenon by virtue of electron transfer from QDs to H_2Q.

5.2 Experimental Section

5.2.1 Materials

L-Cysteine (extra pure 99%) was purchased from SRL chemicals and maleic acid (99%) was purchased from ACROS Organics. For interference study, standard metal ions solutions (conc. 1.0 g/L) of the AAS (atomic absorption spectroscopy) category were purchased from SRL chemicals. Ultrapure water (Milli-Q Ultra-Pure System, Millipore, USA) was used for all synthesis and application parts. All the chemicals were used as such without further purification.

5.2.2 Synthesis of O-and S-doped C_xN_y QDs

O-and S-doped C_xN_y QDs were synthesized by the hydrothermal process using different ratios of cysteine and maleic acid at 150^{o}C.In a typical synthesis, 363.4 mg (3.0 mmol) of cysteine and 58.0 mg (0.5mmol) of maleic acid (6:1 molar ratio) were mixed together and grounded into a fine powder with the help of an agate mortar pestle. This mixed sample was now placed into the hydrothermal bomb and heated at 150°C for 90 minutes. After that, the hydrothermal bomb was cooled to room temperature and brownish char was recovered by dispersing in 100mL of ultrapure water (*see* inset of Fig. 5.1). Thereafter, it was centrifuged into several parts at 4000 rpm for 5 minutes to remove larger non-fluorescent particles, the further purification was carried out by dialyzing it against ultrapure water in a dialysis membrane (MW = 10 k Da) for 48 hrs. This obtained O- and S-doped C_xN_y suspension was labeled as CM61 and kept for further characterization purposes.

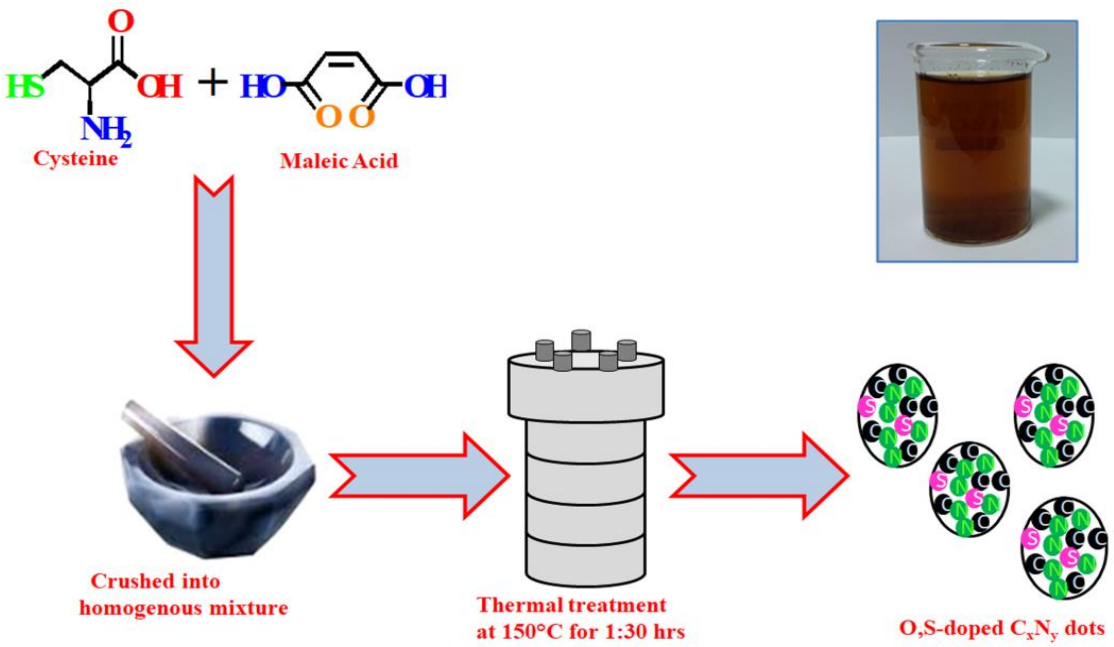

Fig.5.1 Schematic diagram for the synthesis of O- and S-doped C_xN_y QDs. Inset shows aqueous dispersion of as-prepared C_xN_y QDs.

Figure 5.1 summarizes the strategy for the synthesis of QDs. Similar procedures were adopted for the synthesis of CM31, CM91 and CM121 by varying the molar ratios of cysteine and maleic acid in 3:1, 9:1 and 12:1 respectively. Quantum yields of all these as-prepared O- and S-doped C_xN_y QDs are calculated (*see* Table 5.1) with help of the following equations using quinine sulfate (QY = 54.0 % in 0.1M H_2SO_4) as standard.

$$QY_x = \mathrm{QY_{ref}} \frac{\mathrm{I_x\, A_{ref}\, \eta_x^2}}{\mathrm{I_{ref}\, A_x\, \eta_{ref}^2}} \text{.....(Eq. 5.1)}$$

Where, 'QY' stands for quantum yield, 'I' is integrated emission intensity, 'A' is optical density and 'η' is the refractive index. 'X' stands for sample and 'ref.' for reference. (The excitation wavelength and slit width are kept the same for both the standard and prepared samples.)

Table 5.1 Quantum yields of C_xN_y QDs prepared by various molar ratios of precursors.

Sample	**Optical density at λ = 360nm**	**Integrated emission intensity at λ_{ex}=360nm**	**Quantum yield (%)**
Quinine sulphate	0.08	85829	54.00
CM31	0.06	17466	16.65
CM61	0.06	23479	20.08
CM91	0.06	22927	19.30
CM121	0.06	12055	10.99

CM61 has the highest quantum yield of 20.08 % among others due to the homogeneous surface organization. Therefore, this optimized fractional product is extended for other experimentations (as discussed later) and sensing applications; while rest samples were discarded. A comparison of quantum yield of O- and S-doped C_xN_y QDs (CM61) with others reported C-dots and carbon nitride dots has been tabulated in Table 5.2.

Table 5.2 A comparison of quantum yield of doped C_xN_y with other reported C-dots and carbon nitride dots.

System	Quantum Yield (%)	References
CQDs	46.6	D. Bano et al. [201]
N, P-CQDs	73.0	V.K. Singh et al. [202]
N, S-CQD	46.0	V.K. Singh et al. [217]
CNDs	11.0	S. Liu et al. [18]
CNDs	8.9	S. Liu et al. [21]
CNDs	9.0	S. Liu et al. [17]
g-CNQDs	42.0	J. Zhou et al. [22]
g-CNQD	29.0	S. Barman et al. [198]
O, S-Doped C_xN_y	20.08	Present work

5.2.3 Instrumentations

UV-vis spectra and all photoluminescence (PL) spectra were recorded on BioTek EPOCH2 and F-4600 FL Spectrophotometers respectively in 1×1×3 cm^3 cuvette. The vibration spectrum (FT-IR) was recorded from a Thermo Scientific NICOLET iS5 instrument. Field emission scanning electron microscope (FESEM) images were captured on FEI NOVA NANO SEM 450 instrument. Transmission electron microscope (TEM) images were captured on FEI, TECHNAI G2 20 TWIN instrument with accelerating voltage of 200 kV. Zeta potential measurement was carried out on Horiba nanopartica SZ-100 series model. X-ray photoelectron spectroscope (XPS) measurement was performed on Thermo Fischer Scientific ESCALAB Xi+.

5.3. Results and Discussion

5.3.1 Morphological and Structural Characterization

Figure 5.2 (a) is the TEM image of the as-synthesized CM61, it is exemplified that C_xN_y QD is homogeneous in nature and exists in nanometric range. From the corresponding particle size distribution histogram (Fig. 5.2 (b)), it is confirmed that as-prepared QDs size ranging from 1 to 4 nm with the dominancy of particles having 2 nm size. However, the FESEM image in Figure 5.3 shows globular morphologies of relatively larger size due to the agglomeration of dots. On the other hand, energy dispersive spectra (EDS) confirm the presence of O and S as expected as dopant and C and N as part of C_xN_y in as-prepared QDs.

Thereafter, the Absorbance (blue curve) and emission (red curve) properties of CM61 were measured with the help of UV-Visible and PL spectroscopy (*see* Fig. 5.4 a).

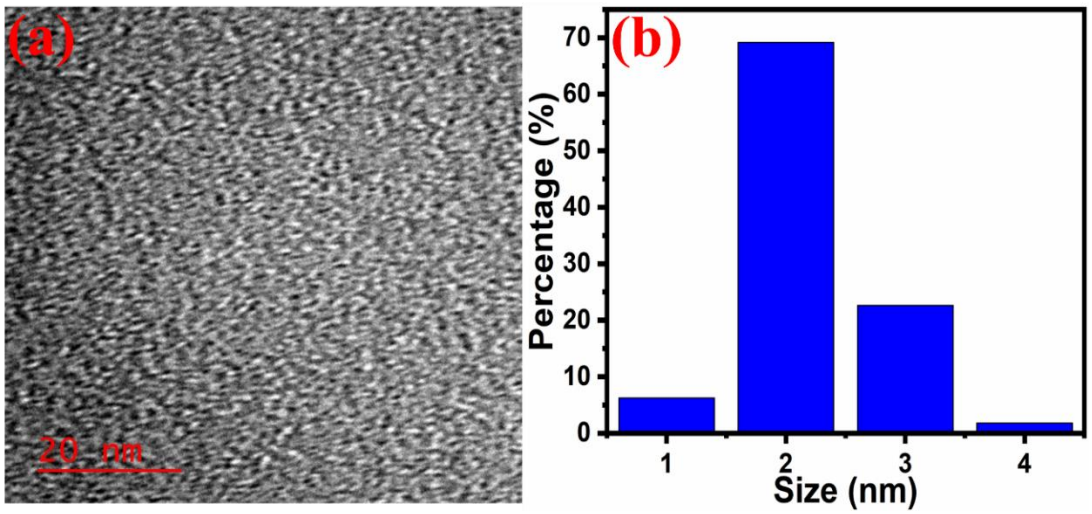

Fig. 5.2 (a) TEM image and (b) the corresponding particle size distribution histogram of CM61.

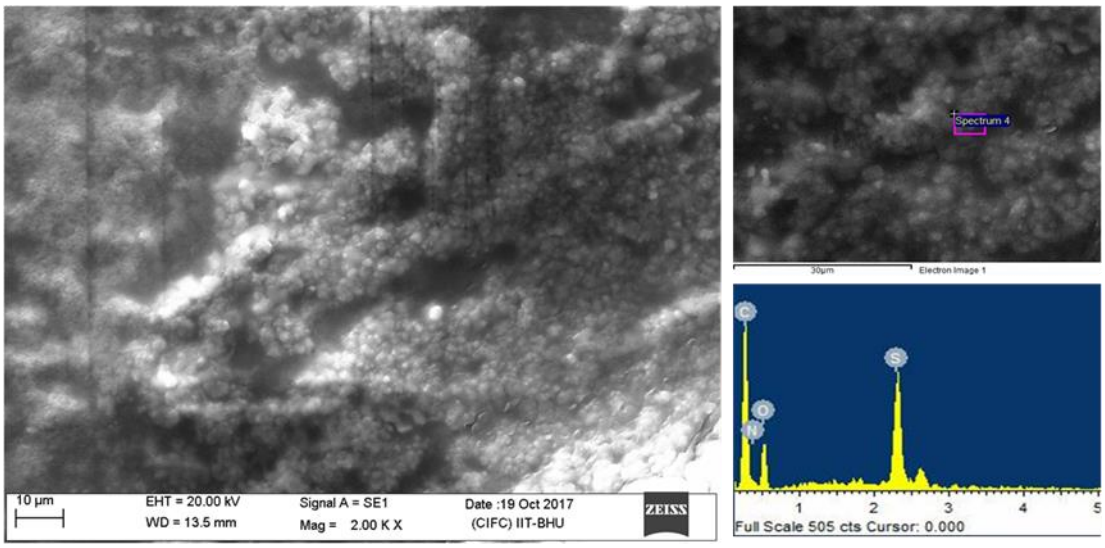

Fig 5.3 FE-SEM image of as prepared C_xN_y QDs and adjacent EDS shows presence of all four elements O, S, C and N in the prepared quantum dots.

The absorbance curve shows a strong absorption peak centered around 280 nm due to n→π* transition chrematistics of C=O. [202,203] Similarly, the emission curve is centered at 439 nm, when excited by 360 nm wavelength. The inset of Figure 5.4 (a) shows photograph of the aqueous dispersion of CM61 QDs when allowed to absorb UV radiation of long-wavelength (365 nm) in the UV chamber exhibiting bright blue color emission.

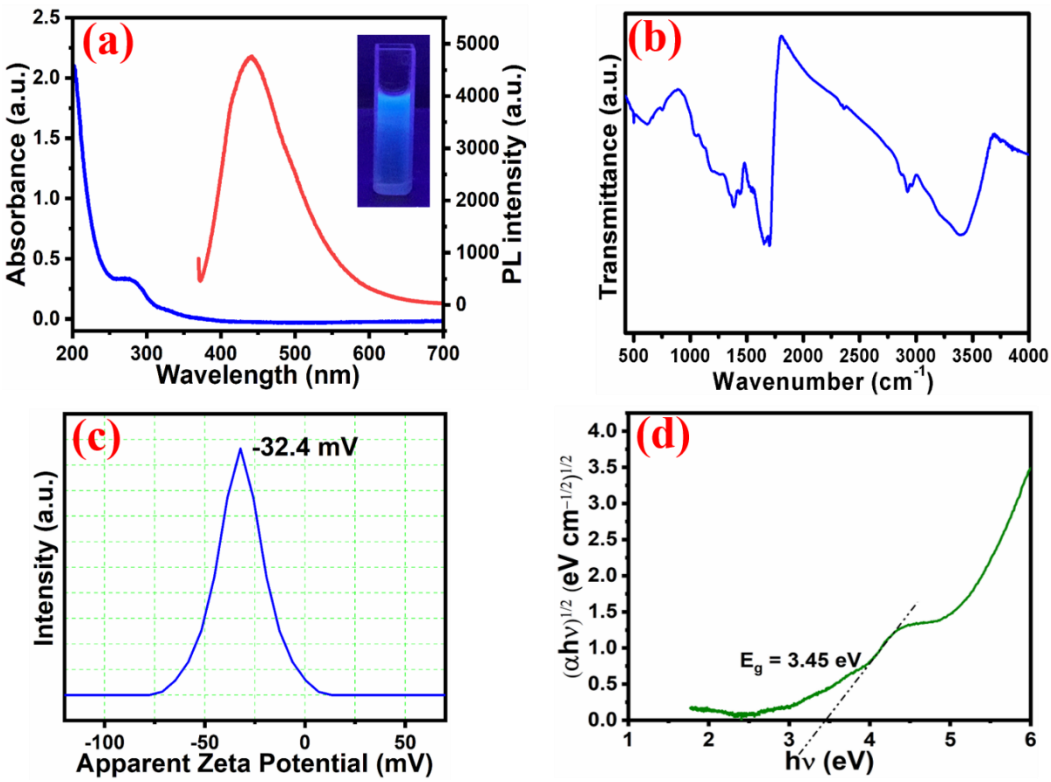

Fig. 5.4 (a) UV-Vis absorbance (blue line) and PL spectra (red line), (b) FT-IR spectrum, (c) zeta potential curve and (d) Tauc's plot for optical band gap of as-prepared CM61 QDs. Inset of Fig. 5.4 (a) shows photograph of CM61 QD dispersion under UV light at wavelength 365 nm.

Vibrational spectra of as-prepared CM61 confirmed the existence of O- and S- as the dopant in C_xN_y (Fig. 5.4 b). The vibration peaks at 757.31 cm^{-1} and 1381.00 - 1709.00 cm^{-1} confirm the presence of various CN units. The small peak at 2358.71 cm^{-1} corresponds to S-H stretching showing a small amount of Sulphur is still present in the C_xN_y dots as the dopant. The peak at 3400.43 cm^{-1} belongs to –OH of maleic acid and some moisture contents in the sample. The vibration peak at 2914.20 cm^{-1} is assigned to -NH_2 stretching mode. [17,198]

The ease of dispersivity was measured by measuring Zeta potentials (*see* Fig. 5.4 c). The value of zeta potential was measured as -32.4 mV which reveals a negative surface charge owing to the presence of $–COO^{–}$,$-O^{–}$ and a small doped amount of $-S^{–}$. [22] This high magnitude of zeta potential causes the stability of the dots in water dispersion even for several months and also imparts significant stability comparable to earlier synthesized quantum dots. The optical band gap for CM61 was calculated to be ~3.45 eV at an absorption edge of 360 nm.

5.3.2 Elemental Analysis in the as-prepared C_xN_y QD

XPS measurement was carried out to ensure the bonding nature of carbon, nitrogen and dopant elements in the prepared material. The survey spectrum (Fig. 5.5 a) confirms the existence of as-expected elements O, S, C and N in QDs. All the corresponding peaks were deconvoluted in order to remark respective bonding states (*see* Fig. 5.5 (b) to 5.5 (e)). C_{1s} peak was deconvoluted into four peaks at 284.3. 285.1, 287.7 and 289.3eV corresponding to C=C, C-C/C-H, C-OH/C-O-C and C=O groups respectively. N_{1s} peak was deconvoluted as pyridinic/pyrrolic N moieties at 399.5 eV, while O_{1s} peak was deconvoluted into two peaks at 531.0 and 531.8 eV corresponding to C-O and C=O bonding state. S_{2p} peak spectrum was deconvoluted into three peaks 163.1, 164.3 and 164.5 assigned to –S-, -C=S- and residual –SH bonding state respectively. [204] Elemental composition determined from peak area integration of XPS survey spectrum shows a significant amount of Sulphur (~8.77 %) and oxygen (~31.85 %) present in the quantum dots.

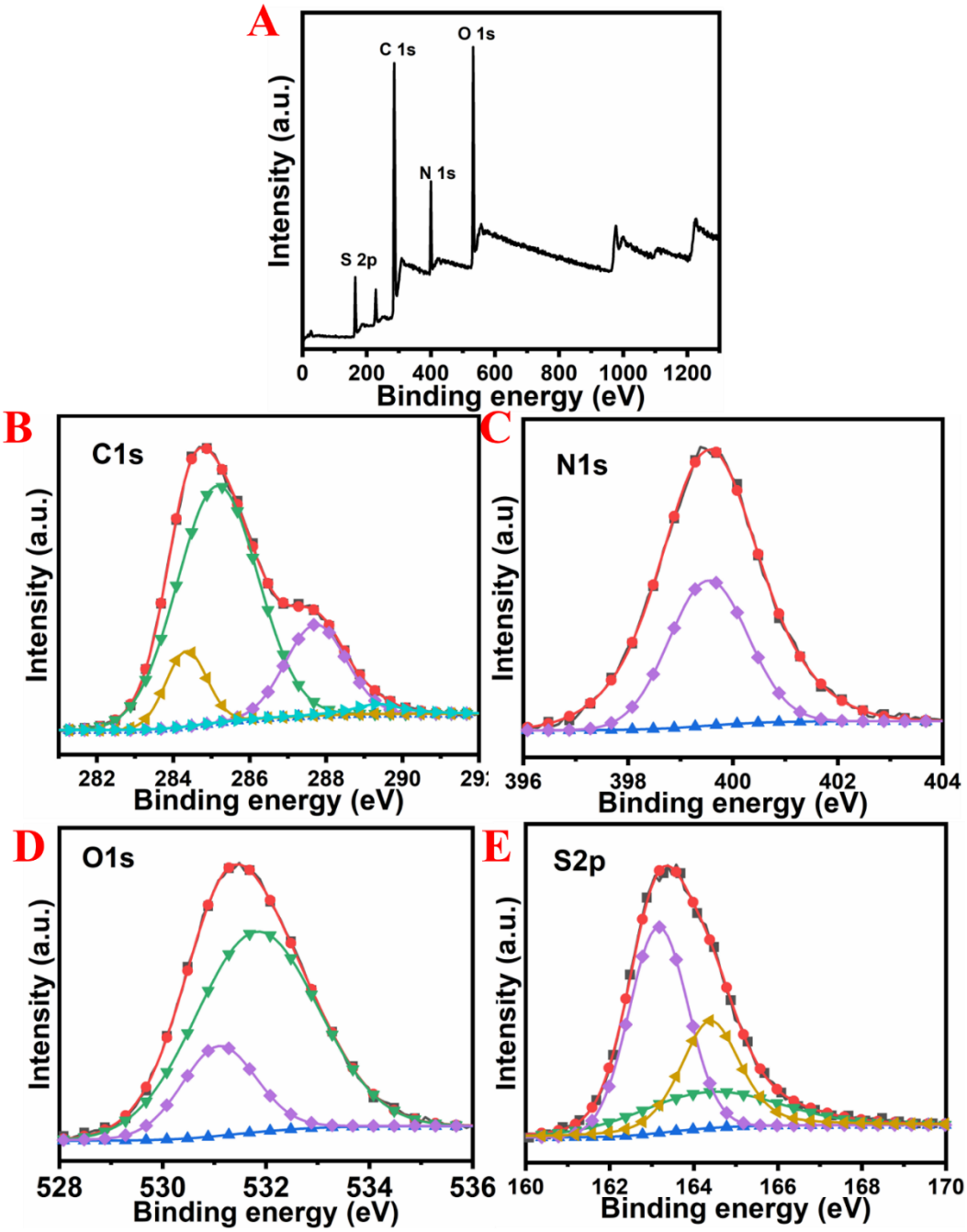

Fig. 5.5 (a) XPS survey spectrum and deconvoluted individual elemental peaks of as-prepared CM61 QD for (b) C_{1s} (c), N_{1s} (d), O_{1s} and (e) S_{2p}.

5.3.3 Optimization of PL Activity

5.3.3.1 Excitation Dependent PL Intensity of QDs

Excitation-dependent PL spectrum was recorded in order to study the optical properties of the as-prepared QDs. We found that emission peaks shift its position and intensity upon excitation of the sample at various excitation wavelengths from 280 nm to 420 nm. The emission peaks first shift to a shorter wavelength with an increase in intensity below 340 nm. However, after this excitation wavelength, the peak position shifts to a higher wavelength with a decrease in intensity (*cf*. Fig 5.6 a and 5.6 b). Since, we are getting the highest emission peak intensity at excitation wavelength 360 nm, this excitation wavelength is further used for all H_2Q detection parts. Such behavioral of emission spectra is attributed to various surface energy traps present on the surface of QDs and the suggested mechanism for luminescence is based on radiative recombination of excitons. [205, 206] Apart from this, large surface-to-volume ratios also play the role for strong photoluminescence of as-prepared QDs that led to quantum confinement of emissive energy traps to the particle surface. While in the case of larger particles there is the absence of photoluminescence owing to a small surface to volume ratio.

5.3.3.2 pH Dependence of PL Intensity of QDs

The dependency of PL intensity was further checked by varying the pHs of aqueous dispersion media. There is not much variation in PL intensity of QDs was observed on varying pH of the solution. Although at pH 7.0, we observed better intensity maxima (*cf*. Fig 5.6 c and 5.6 d). Similarly, long term PL stability of as-prepared QDs were tested by continuously irradiating the sample kept in cuvette under a UV lamp

(λ = 365 nm) for the time period of 6 h as shown in Figure 5.7 We did not get any variation in PL intensity, which implies its long-term PL stability under exposure conditions.

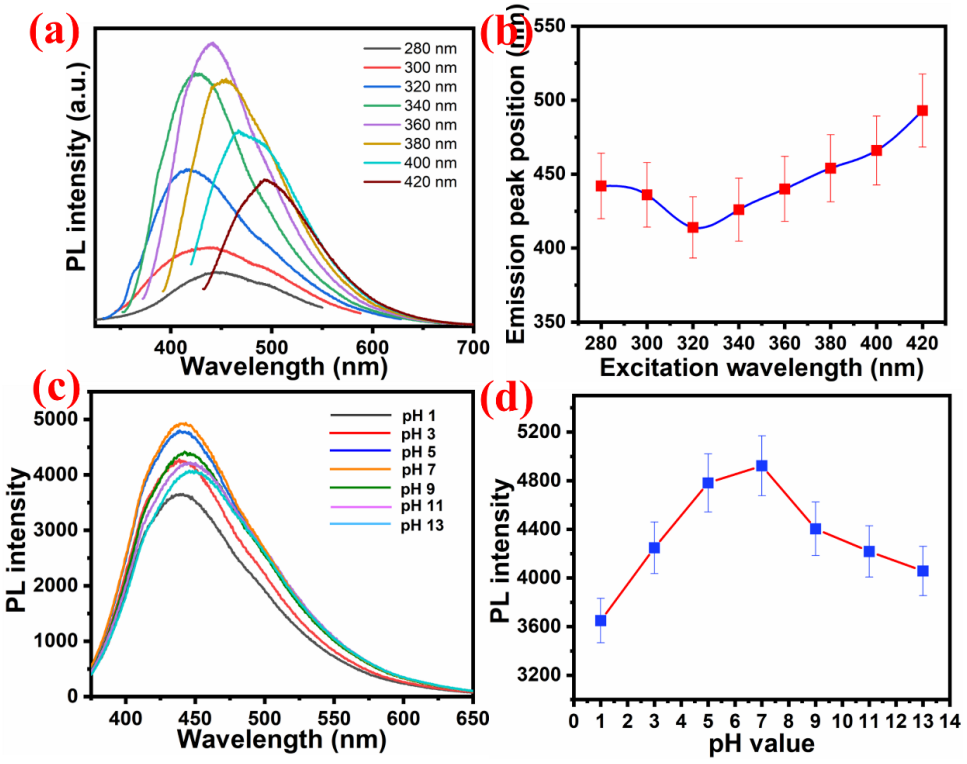

Fig. 5.6 (a) Emission spectra of CM61 at excitation wavelengths from 280 nm to 420 nm, (b) plot of emission peak position corresponding to excitation wavelength, (c) PL intensity of CM61 at various pHs and (d) variation of PL intensity with pH value.

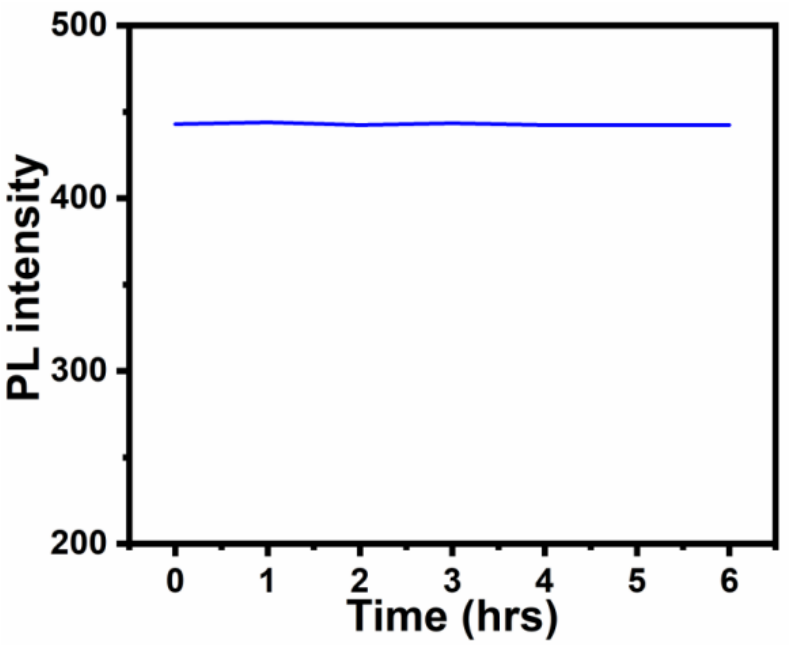

Fig. 5.7 PL emission intensity of prepared sample under continuous irradiation of UV light (365nm).

5.3.3.3 Control Experiment

A control experiment was performed in order to check the individual role of cysteine and maleic acid in the synthesis and PL activity of C_xN_y QDs. For this, first of all, maleic acid and cysteine were heated individually at the same temperature and same time period (as explained in the synthesis section). In cysteine, little charring was observed, while maleic acid melts at the end of experimental conditions. Both these samples have no fluorescence activity under the above conditions. After that, the mixture of these precursors in 6:1 molar ratio was again kept as such at room temperature for 48 h. No reaction takes place at the end of experimental conditions, which justifies the role of heat treatment in the preparation of O- and S-doped C_xN_y QDs. As per the above exemplifications, we choose 360 nm as excitation wavelength,

aqueous dispersion agent having pH = 7.4 and CM61 as-prepared QDs for H_2Q sensing alone or in presence of interfering media.

5.3.4 H_2Q Detection by PL Quenching

5.3.4.1 H_2Q Detection

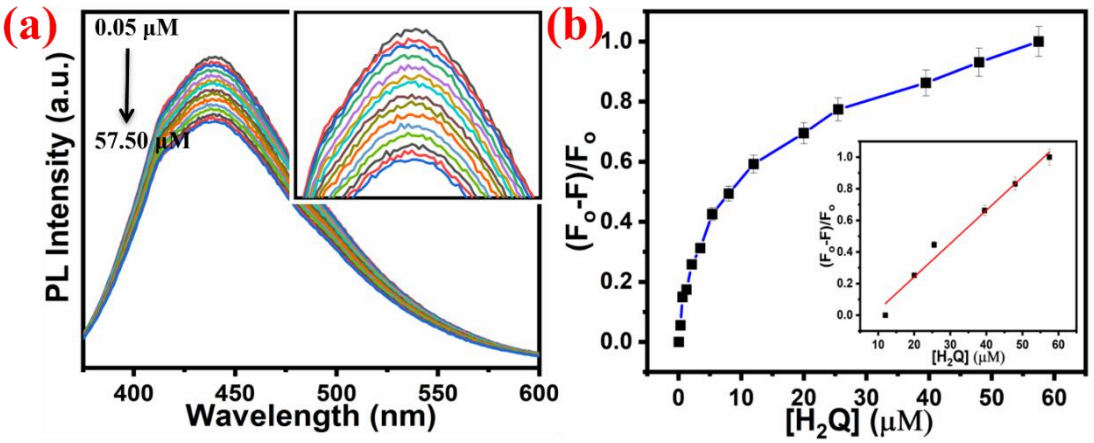

Fig. 5.8 (a) PL emission spectrum of CM61 upon addition of various concentrations of H_2Q solution; Inset of Fig. 5.8 a show the zoomed part of the reduction in PL intensity and (b) relationship between $(F_o\text{-}F)/F_o$ and concentration of H_2Q; Inset of Fig. 5.8 (b) exhibits the linear calibration plot in the range of 12.0 to 57.5 µM.

The detection of carcinogenic pollutant H_2Q was performed with the help of as-prepared O- and S-doped C_xN_y QDs by photoluminescence quenching phenomenon. All the detection experiments were performed in 7.4 pH phosphate buffer solution (PBS). Excitation and emission slit width was kept at 5.0 nm for all runs. For a typical detection, 2ml PBS buffer was taken and a certain amount of fixed

concentration of QDs was added into it. Thereafter, the various concentration of H_2Q was spiked into it and PL intensity was recorded from the instrument at excitation λ=360 nm. For the interference test, an individual run was carried out with the individual addition of interfering agents; a similar method was adopted for real sample analysis.

To ensure the reliability of the result, all the measurements were performed in triplicate at room temperature. Figure 5.8 (a) show the variation in PL intensity of O- and S-doped C_xN_y QDs upon addition of different concentration of H_2Q solution from 0.05 µM to 57.05µM (0.05, 0.33, 0.64, 1.28, 2.13, 3.48, 5.38, 8.0, 12.0, 20.0, 25.5, 39.5, 48.0 and 57.5µM). Herein, it was observed that the PL intensity of C_xN_y QDs is directly related to H_2Q concentrations. Figure 5.8 (b) shows the relationship between PL quenching in terms of $(F_o\text{-}F)/F_o$ and H_2Q concentration, where F_o is PL intensity in absence of H_2Q and F is PL intensity in presence of H_2Q. Inset of Figure 5.8 (b) is linear calibration plot for H_2Q detection in the concentration range of 12.0 to 57.5 µM. The linear regression equation obtained is $(F_o\text{-}F)/F_o$ = -0.070 + 0.021 [H_2Q] (µM) with correlation coefficient of 0.9793. Limit of detection (LOD) is calculated as three times of standard deviation (S/N = 3), divided by the slope of the linear fit (as quoted in Eq. 1.19 in the section 1.4.5.2(d)). The obtained LOD is 50 nM which is comparatively good to another electrochemical and fluorometric detection method of H_2Q as listed in Table 5.3. This detection limit is significantly lower than the bar (0.5 mg/l) set by the US Environmental Protection Agency for the discharge of phenolic pollutants into water. Table 5.3 sums up the limit of detection (LOD), linear range, the system deployed and techniques used along with references for detection of H_2Q. It is clear that our proposed system has impressive sensitivity in the detection of H_2Q.

Table 5.3 Comparison of different methods for detection of H_2Q.

Methods	System	Linear range (µM)	LOD (µM)	Ref.
Electrochemistry	Graphene	1-10 and 10-80	0.8	S.-J. Li et al. (2012) [207]
Electrochemistry	PEDOT-NGE	1.0-10	0.18	W. Si et al. (2014) [208]
Electrochemistry	GQDs	4.0-600	0.40	X. Jian et al. (2016) [209]
Electrochemistry	Co_3O_4-His-GQD	0.002–800	0.00082	H. Wang et al. (2017) [210]
Electrochemistry	Pt-graphene	20-115	12	J. Li et al. (2011) [211]
Fluorometry	CdTe QDs-enzyme	0.5-500	0.5	J. Yuan et al. (2008) [212]
Fluorometry	C-dots	0.1-50	0.1	P. Ni et al. (2015) [213]
Fluorometry	GQDs	0.01-30	0.005	Y. He et al. (2015) [214]
Fluorometry	g-CNQDs/H_2O_2-HRP	0.5-11.6	0.04	J. Chen et al. (2019) [20]
Fluorometry	$PPESO_3$-enzyme	1.0-200	0.5	H. Huang et al. (2011) [215]
Fluorometry	Doped Carbon nitride (C_xN_y)	12-57.5	0.05	Present work

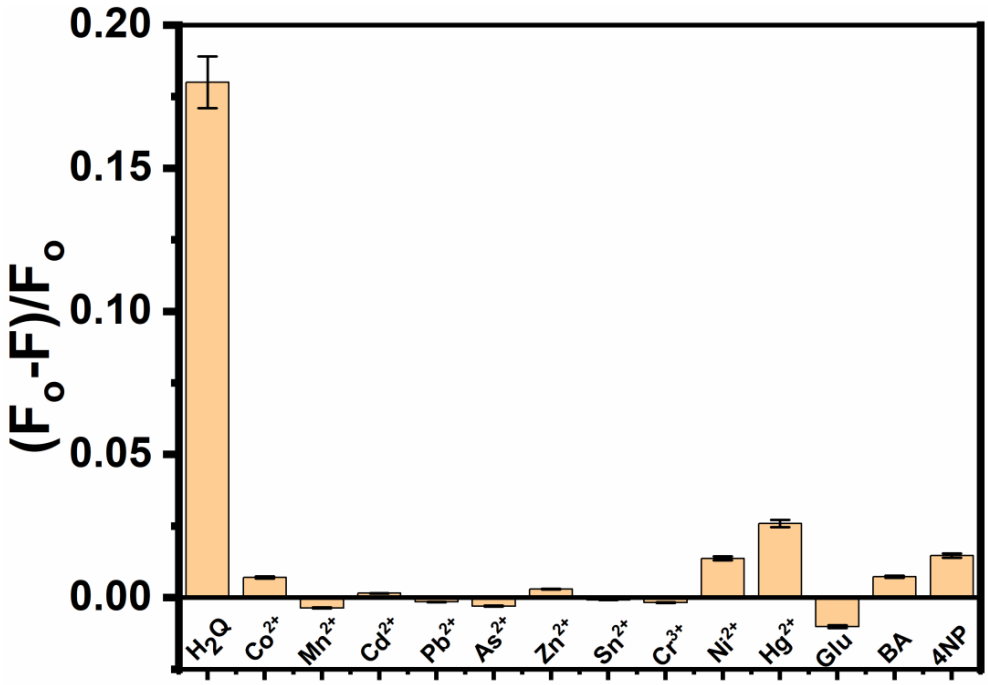

Fig. 5.9 Selectivity of the CM61 for 8 µM H_2Q detection in presence of various interfering agents. [Concentration of metal ions Co^{2+}, Mn^{2+}, Cd^{2+}, Pb^{2+}, As^{2+} and $Zn^{2+}$are 1 g/l; Sn^{2+}, Cr^{3+} and Glu have concentrations of 5 mM; $Ni^{2+}$and Hg^{2+}have concentrations of 0.1 g/l; o-Amino benzoic acid (BA) and 4-Nitrophenol (4NP) have concentrations of 0.05 mM]

5.3.4.2 Selectivity of O- and S- doped C_xN_y QDs and Real Sample Analysis

Selectivity of any sensor is an important parameter to test the onsite samples due to the presence of various contaminants that might inhibit the existing sensing performance. We investigated the selectivity of as-prepared QDs for the detection of H_2Q (8 µM) against a series of potential interfering ions and compounds found in wastewater. Interfering ions chosen are Co^{2+}, Mn^{2+}, Cd^{2+}, Pb^{2+}, As^{2+}, Zn^{2+}, Sn^{2+}, Cr^{3+}, Ni^{2+}, $Hg^{2+}$and compounds are Glucose, o-Amino benzoic Acid (BA) and 4-Nitro phenol (4NP). Potential interfering agents (Ni^{2+} and Hg^{2+}) diluted to 10 times show a

small interference as compared to others. As seen in Figure 5.9, PL activity of as-prepared C_xN_y QDs has almost no impact on the presence of interfering agents during selective sensing of H_2Q. Hence, as-prepared QDs show highly selective quenching of pollutant H_2Q in presence of other interfering agents, which enhances its probability to be chosen as a potential candidate for H_2Q detection in real samples.

Table 5.4 Determination of H_2Q in real samples.

Sample	Added (μM)	Found (μM)	Recovery (%)	RSD (%) n=3
Ganga Water I	5.0	4.90 ± 0.02	98.0	3.32
Ganga Water II	5.0	4.97 ± 0.03	99.4	2.65
Pond Water	5.0	5.10 ± 0.02	102.0	3.19
Tap Water	5.0	4.96 ± 0.05	99.2	3.42

To test the feasibility of the as-prepared QDs in real-life sensing system for detection of H_2Q, we used four real samples in this regard namely Ganga Water I (collected from Ganga River, Haridwar), Ganga Water II (collected from Ganga River, Assi, Varanasi), Pond water (collected from the pond near director office, IIT-BHU) and Tap water from (available in lab). We diluted these real samples ten times by adding pH = 7.4 PBS buffer into it and spiked 5 μM of H_2Q into it. Table 5.4 shows the H_2Q amount found in the real samples with % recovery and relative standard deviation for triplicate measurements. From this table, it is exemplified that our as-prepared QD is successfully able to intentionally added H_2Q in all real samples.

5.3.4.3 Possible Detection Mechanism

Fluorescence-based quenching is obtained either because of static quenching, dynamic quenching, photoinduced electron transfer (PET), resonance energy transfer (RET), charge transfer (CT), electrostatic interactions, hydrogen bond interactions and pi-pi interactions or a combination of these. [216] In earlier reported research work, the mechanism of fluorescence quenching of QDs based sensing system is attributed to fluorescence resonance energy transfer (FRET), electron transfer (ET) or other interactions at the surface of dots. [212] Since, the absorption spectrum of H_2Q does not overlap to the emission spectrum of as-prepared C_xN_y QDs, so the possibility of FRET is ruled out (*see* Appendix A Fig. A.7). In our case, we propose that the photoluminescence quenching of QDs, upon introduction of H_2Q, is due to electron transfer occurring from QDs to oxidized H_2Q via $-S^-$ and $-COO^-$ groups available at the QDs surface, which results in the reduction of PL intensity. H_2Q remains oxidized into benzoquinone (BQ) in alkaline 7.4 pH PBS buffer by dissolved oxygen in presence of QDs. [214] Actually, in this process, it has been interpreted that upon adhering of BQ to QDs'surface, BQ acting as e^- acceptor promotes electron transfer from the conduction band of QDs to its valence band resulting in quenching of PL intensity. Figure 5.10 shows the schematic illustration of the mechanism involved in the detection of H_2Q by prepared C_xN_y QDs. The role of dissolved oxygen is apparent as a quenching study was performed in N_2 saturated PBS buffer solution as shown in Appendix A Figure A.8.

Our proposed method of detection of H_2Q has an edge over earlier reported methods in terms that here doped C_xN_y QDs senses H_2Q directly without the help of any enzyme or polymer assisted system with the detection limit of 50nM in the linear

range of 12.0 to 57.5 µM. The sensing material QDs were prepared in one step and shows the stability of several months. The proposed sensing system also shows a high level of H_2Q sensing in different real water samples with an RSD of 3.15 %.

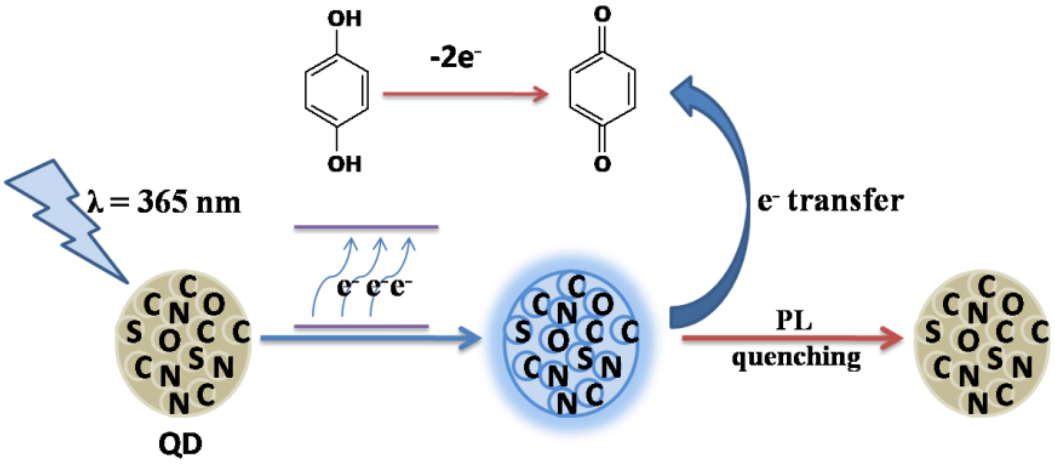

Fig. 5.10 Plausible mechanism of H_2Q detection using CM61 QDs.

5.4 Conclusions

In summary, we have successfully synthesized highly stable photoluminescent O- and S-doped C_xN_y QDs which is efficient for sensitive and selective detection of H_2Q at the detection limit of 50nM. It shows detection of H_2Q by electron transfer mechanism between QDs and H_2Q that result in quenching of PL intensity of dots. The as-prepared QDs dispersion is stable for months owing to a high zeta potential value of -32.4 mV. At the same time, the PL intensity of QDs is stable in various pH values and under continuous exposure to UV light. The effectiveness of detection was

tested in the presence of various potential interfering ions and compounds. A real sample test was also done to check the reliability of the proposed method and the result obtained are 98-102 % range of recovery with 3.15% of relative standard deviation. The proposed system is facile in synthesis, highly stable, sensitive and selective for detection of pollutant H_2Q in real-life samples.